X-625-76-108
PREPRINT

NASA TM X- 71130

AURORAL VECTOR ELECTRIC FIELD AND PARTICLE COMPARISONS

1. PRE-MIDNIGHT CONVECTION TOPOLOGY

N. C. MAYNARD
D. S. EVANS
B. MAEHLUM
A. EGELAND

MAY 1976

GSFC — GODDARD SPACE FLIGHT CENTER
GREENBELT, MARYLAND

(NASA-TM-X-71130) AURORAL VECTOR ELECTRIC FIELD AND PARTICLE COMPARISONS. 1: PRE-MIDNIGHT CONVECTION TOPOLOGY (NASA) 35 P HC $4.00 CSCL 04A

N76-25711

UNCLAS
G3/46 43643

Auroral Vector Electric Field and Particle Comparisons

1. Pre-midnight Convection Topology

N. C. Maynard[1]
D. S. Evans[2]
B. Maehlum[3]
A. Egeland[4]

May 1976

1. Laboratory for Planetary Atmospheres
Goddard Space Flight Center, Greenbelt, Maryland 20771
2. Space Environment Laboratory
NOAA, Boulder, Colorado 80302
3. Norwegian Defense Research Establishment
P. O. Box 25, Kjeller, Norway
4. Norwegian Institute for Cosmic Physics
P. O. Box 1038, Blindern, Oslo 3, Norway

ABSTRACT

Polar 3 (a Nike-Tomahawk) was launched from the Andøya Rocket Range in northern Norway on January 27, 1974. Traversing nearly 3° of latitude, the rocket crossed over a stable IBC II auroral arc in the positive bay region and continued north to a convection boundary which has been identified as the Harang discontinuity. Measurements of the complete electric field vector, of energetic electrons and of the auroral N_2^+ (4278 Å) and OI (6300 Å) emissions have been used to study the convection topology in the pre-magnetic-midnight region. The electric field was mainly northerly (about 60 mV/m south of the auroral arc and 20 mV/m or less elsewhere) over most of the flight, rotating to the west in the region of the Harang discontinuity. No evidence of electric fields parallel to the magnetic field was seen throughout the flight. A strong anticorrelation was observed between the electric field and the precipitating energetic electrons as the rocket passed over the auroral arc. The inverted V nature of the electron precipitations at the convection boundary, compared with the lack of such structure over the arc which was within the positive bay region, leads to the conclusion that auroral arcs are likely to be associated with inverted V type precipitation only at or poleward of convection boundaries and their eddy structures.

I. Introduction

Electric field measurements from which all three components can be obtained have been rare (see Kelley et al., 1975). For this reason comparisons of electric fields and other relevant auroral parameters have generally been limited to where only one component of the electric field is known or where the electric field vector within the spin plane of a rocket is known. From such comparisons anti-correlation of electric fields and precipitating particles have sometimes been observed (i.e. Aggson, 1969; Maynard et al., 1973) and sometimes not observed (i.e. Mozer and Fahleson, 1970). "Inverted V" structures of precipitating particles (Frank and Ackerson, 1971) have been correlated with electric field boundaries or reversals (Frank and Gurnett, 1971) and with auroral arcs (Ackerson and Frank, 1972).

In addition, an overall picture of the high latitude, electric field driven convection patterns has evolved from various measurements of electric fields (Ba^+ releases, single axis double probe measurements on satellites, double probe measurements on rockets, ground backscatter radar measurements, etc.). Near magnetic midnight the negative bay region overlaps the positive bay region on the poleward side. The electric field changes from basically northerly in direction in the positive bay region, through the west, to a southerly direction in the negative bay region as one crosses this boundary called the Harang discontinuity (see Maynard, 1974). In the vicinity of this boundary details of the electric field are sketchy due to the lack of complete knowledge of the electric field vector in previous measurements.

A sounding rocket launched in a northerly direction at low inclination can be used to provide a spatial profile of parameters across several degrees of latitude. In this paper we report on results from electric field, auroral particle and photometer (optical) measurements over nearly three degrees of latitude in the positive bay region near magnetic midnight. The overall topology of the electric field and particle precipitation and its relation to the auroral conditions as seen from the rocket and the ground will be presented. A companion paper (Evans et al., 1976) will explore in more detail the ionospheric effects of the relationship between precipitating particles and electric fields in the vicinity of a IBC II auroral arc.

II. Flight Performance

Polar 3 (a Nike-Tomahawk) was launched at 19:08:46 GMT on January 27, 1974, from the Andøya Rocket Range in northern Norway (69° 17' 40" N and 16° 01' 22" E geographic). A low launch elevation (72°) resulted in a large horizontal flight range. Between traverses of the 100 km altitude level 2.9° of latitude were crossed. Apogee was at 242 km. The trajectory was obtained using data from a tone ranging system. A gyroscope reference platform measured the attitude of the rocket with an accuracy of between 1 and 2° considering errors both from the gyro and mechanical misalignment. Final spin and precession periods were 1.575 and 154 s, respectively.

The flight traversed over a "stable" auroral arc to the north of Andøya with an intensity of IBC II. Magnetic local time was 22.0 hours at launch; hence, the flight was likely into a positive bay type pre-magnetic-midnight condition. A more comprehensive discussion of the auroral and magnetic conditions is found in Section III.

The instrument complement included a two axis electric field measurement (capable of resolving all three components), low energy particle detectors (channeltrons covering electrons from < 0.1 to 16 keV), tilting narrow bandwidth photometers covering the N_2^+ (4278Å) and O1 (6300Å) emissions, and a Langmuir probe for electron density measurement. Data from the first three instruments will be presented here.

III. Ground Observations

Figure 1 shows three all-sky photos taken from the launch site at 40, 240 and 440 s during the flight. The basic arc structure which at a point east of Andøya curled back to the northwest existed for some time prior to launch and also continued in approximately the same location for a significant period after the launch. The positions of the magnetic field lines at 110 km which intersect the rocket trajectory at 150, 230 and 380 s are shown on the respective photos. As will be subsequently shown, 150 and 230 s are the entry and exit times from the arc as determined from data gathered by the onboard charged particle and photometer instruments. The intensification of the arc in the vicinity of the trajectory seen in the 240 s photo was not present in the photo taken at 150 seconds (at the time of entry into the arc). At that time the whole arc as seen by the all-sky camera was of nearly uniform intensity. The variations in intensity in the 240 s photo developed to the east and drifted west in subsequent photos. After 340 s electron fluxes were again of sufficient intensity to create visual aurora. Note that during the flight the main arc is slowly moving southward. This can be seen relative to the positions of the star Vega located just above the 3 in 230 in the middle photo, and just above

and to the right of the 0 in 380 in the bottom photo. The position of the northward form is also moving southward and the 380 s point falls within the emission recorded on the 440 s photo. From scaling the all-sky photos, the average southward velocity of the main arc during the flight was a little over 100 m/s while the southward velocity of the second arc was between 300 and 500 m/s.

The launch occurred during the recovery from a large substorm over the northern regions of the Soviet Union (maximum negative ΔH at Tixie Bay had been over 800γ). Figure 2 shows magnetogram records from the magnetic observatories at Tixie Bay, Dixon Island, Murmansk and Tromsø, and from the range magnetometer at Andøya. The polar diagram in the upper right shows the positions of the stations in magnetic time-invariant latitude coordinates at the time of the launch (T = 0 line on the magnetograms). The line from Andøya represents the horizontal range covered by the rocket. Horizontal magnetic disturbances are shown for the Soviet stations. The horizontal disturbance at Tromsø was essentially zero. The horizontal disturbance at Andøya is somewhat anomalous in changing from southeast to northeast during the flight. There is no simple horizontal current system that can give this initial southward ΔX at Andøya with Tromsø zero and Murmansk southward. Local structure and/or field aligned currents must be involved. The conclusion is that the Harang discontinuity (see Maynard, 1974) must be in the vicinity of these stations at launch time. Chen and Rostoker (1974) associated a negative ΔD extending from low to high latitude with the Harang discontinuity, a condition satisfied in the vicinity of Tromsø around the time of flight and earlier at Murmansk. The earlier large positive ΔD nearer 1800 hours

is associated with the westward travelling surge from the substorm. Andøya is clearly positive in ΔD through the flight.

IV. On Board Photometer Measurements

Two narrow-band tilt-filter photometers were mounted at 135 degrees to the rocket axis to look down on the aurora. The tilting motion of the interference filters caused the photometers to scan the two wavelength regions 6284 - 6310 and 4254 - 4286Å some five times every second, and the bandwidth of the filters was 6 - 7Å. Hence, we monitor both OI (6300Å) and N_2^+ (4278Å) emissions and the "background" emissions on adjacent wavelengths every 0.2 s. The onboard optical observations presented refer to intervals when the photometers were looking less than 15 degrees off the geomagnetic field lines downwards, and the "background" emissions have been subtracted from the data.

The rocket photometers detected a luminous region beginning near 160 s, and passed the northern boundary of the auroral display near 220 - 230 s. The "rugged" structure in the luminosity is partly caused by variations in the looking direction relative to the local geomagnetic field vector. These variations also introduce an uncertainty in the location of the auroral display. An offset of 10 degrees in the viewing direction relative to the geomagnetic field vector corresponds to an uncertainty of up to 15 s in the flight time near 150 s.

The total intensity of the 4278Å band, corrected for filter bandwidth is 3 kR between 160 and 220 s. The total energy influx of precipitated electrons required to produce a 3 kR intensity is some 20 erg cm^{-2} s^{-1} (Rees and Luckey, 1974; Gustafsson and Egeland, 1976)

which is 30% less than the data to be presented in Figure 4. This is well within the absolute calibration errors of the instruments. The observed intensity of the 6300Å line emission is around 1 kR, giving a 6300Å/4278Å ratio of 0.3. As seen from Figure 3 fairly large variations in this ratio occur during the flight. According to Eather and Mende (1971) this ratio is normally 1 - 2 deduced from ground observation in the auroral zone. We therefore conclude that the main part of the 6300Å emission is located above the rocket, i.e. above 230 km altitude.

The maximum intensity of about 3 kR of the 4278Å band corresponds to 10 - 15 kR of λ 5577Å. The observed intensities from ground based photometers at Andenes were 1.2 kR and 5 kR, respectively. Since the arc was located at an elevation of 26 - 28°, the "true" intensity viewed along the field line may have been twice these values, in good agreement with the rocket data.

V. Electron Measurements

Detailed observations were made of the auroral electron fluxes over the energy range from < 0.1 to 16 keV using electrostatic-analyzer channel-multiplier detector systems. Four individual detector units of a design similar to those described by Hoffman and Evans (1967) were flown onboard Polar 3. These detectors were mounted in pairs, one pair viewing upwards at 45° and the other pair downwards at 135° to the rocket spin axis. This mounting arrangement, together with the spin of the rocket, allowed electron pitch angle distributions to be measured over a large range in angle, often from ≃ 0 to ≃ 180°.

Each detector in the pair was swept in energy through separate but

overlapping energy ranges. The time required for an energy sweep was .131 s. This time coupled with the rocket spin period allowed a complete intensity-energy-pitch angle data set to be gathered in 1.57 s.

Intercomparisons between the four detector responses during those periods when all four sampled electrons of the same energy and pitch angle within a time of 0.8 s showed agreements amongst detectors to within ± 15%. The uncertainties in the absolute flux values derived from the detector responses is estimated to be within ± 40% from uncertainties in detector efficiencies, geometries and shape of the energy passbands.

Figure 4 displays the total electron energy flux incident upon the atmosphere during the flight. These values were obtained from a numerical integration of the data over pitch angle and from 0.5 to 16 keV. The detector responses were well above background at all times.

The region of greatly enhanced energy flux between 150 s and about 230 s defines the extent of the auroral arc sampled by this flight. A typical differential-directional electron energy spectrum taken above this aurora is shown in Figure 5. The spectrum is relatively flat over the energy range 0.6 to 7 keV, but falls sharply at higher energies. While there is no great evidence for a monoenergetic peak in this spectrum, the change in slope at 7 keV does demark a characteristic beam energy. It was also observed that over this aurora the pitch angle distribution of the precipitating electrons was isotropic to within a factor of 2 at all electron energies. We find no evidence of field aligned beams between 0.1 and 16 keV above this auroral arc.

It should be pointed out that the spatial variation in the electron precipitation as the rocket approached and passed over the auroral form

did not reproduce the inverted V pattern. There was no characteristic energy variation in the electron beam over the spatial scales observed in inverted V's by satellite instrumentation (Frank and Ackerson, 1971). Instead the electron precipitation flux simply increased in the energy range 4 - 8 keV in a spatial scale size of 5 km.

The scatter of data points seen in Figure 4 between 240 and 270 s were due to a number of very short lived but intense electron events. The origin of these short lived events is unknown and their discussion is outside the scope of this paper.

After 310 s into the flight, the energy flux carried by the electron precipitation once again began to increase, reaching sufficient intensity to cause visual aurora at about 340 s. In this region of precipitation the electron pitch angle distribution was moderately field aligned. The nature of the electron energy spectrum (Figure 6), and the spatial scale over which the electron average energy monotonically increased all suggest that this precipitation was of the inverted V type. The payload re-entered the atmosphere at 390 s before the entire inverted V structure was traversed. A further discussion of the particle measurements, their effect upon the ionosphere, and detailed analysis of the electron, electric field, and ionospheric behavior in and near the arc is given in a companion paper (Evans et al., 1976).

VI. Electric Field Measurements

The electric field data presented here are from a two axis measurement utilizing the double probe technique (Aggson, 1969). The four long cylindrical antennas (each 10 feet long with the outer 2 feet comprising

the active probe area) were directed at 45° or 135° to the spin axis in a plane containing the spin axis. The resulting baseline for the measurements is 5.8m on each axis. In this configuration as the rocket rotates, a new measurement of all three components of the electric field is possible every 180° of rotation. On each axis the resulting signal, V, over a spin period is made up of a sinusoid from a fraction of the spin plane electric field and a constant consisting of the sum of a fraction of the spin axis electric field and contact potential differences. This V can be expressed by

$$V = [\vec{E}_{sp} \cos(\lambda) \sin(\omega t + \phi) + \vec{E}_{sa} \sin(\lambda)] \cdot \vec{d} + V_{c1} - V_{c2},$$

where $\vec{E}$ ($\vec{E}_{sp} + \vec{E}_{sa}$) is the vector sum of the ambient field and $\vec{v} \times \vec{B}$, λ is the angle between the measurement axis and the spin plane, ω is the spin rate, $\vec{d}$ is the vector baseline, ϕ is the phase of $\vec{E}_{sp}$ in the spin plane, and V_{c1} and V_{c2} are the contact potentials. The angle λ in practice will be less than 45° due to the centrifugal bending of the antennas toward the spin plane. The expressions for the two axes will differ only by 180° in ϕ and in different contact potentials.

The data from each axis were fitted by a sliding least squares technique (one spin cycle of data for each fit with 1/8 cycle slide) to separate out the sinusoidal component from the constant component. A contact potential difference for each axis then had to be assumed and subtracted from the constant component. To construct an orthogonal 3 component measurement at any particular time, the two components of the electric field along the theoretical measurement axes (at 45° to the spin

axis) were determined using the least squares fit data and also correcting for contact potential differences and antenna bending. The third orthogonal component was determined by calculating the electric field measured by each axis 90° in spin later in the same manner and dividing the difference by 2 cos (45°).

Attitude of the rocket was measured by a gyroscope reference system. A transformation matrix to convert from topographic coordinates to the rocket coordinate system was calculated and used to transform $\vec{v} \times \vec{B}$, calculated from the trajectory (derived from tone ranging data) and a theoretical $\vec{B}$ (POGO 8-68 model $\vec{B}$), into the rocket system. After the vector subtraction of $\vec{v} \times \vec{B}$ from the measured components, the resulting electric field was then transformed back to topographic coordinates using the inverse of the gyro derived matrix. A further transformation was made into a magnetically oriented system in which the Z axis is down and along $\vec{B}$, the X axis is perpendicular to Z and in a plane containing Z and the direction of the maximum horizontal component of $\vec{B}$ (approximately north), and the Y axis completes the orthogonal system (approximately east). The rotation of the XZ plane with respect to geographic north increases from 1.4 to 3.6° west of north over the flight as the distance from Andøya increases.

Contact potentials were adjusted by minimizing variations with periods of the spin period, 1/2 of the spin period, the precession period and 1/2 of the precession period from the resultant data. It was assumed that the contact potentials were constant or slowly varying so that they could be represented by constants or linearly varying functions over significant

portions of the flight. The resultant contact potentials are shown in Figure 7. The amount of antenna bending was also checked using the same minimizing criteria. A value for λ was set at 44° which indicated less than the expected amount of bending by about 2°.

The electric field data are presented in Figure 8. All data are in the magnetically oriented system described above. The upper half shows the total perpendicular electric field and its azimuth versus time. The lower half depicts all three components. Note that invariant latitude contours are canted in the topographic system at an azimuth of about 75°. Thus, in this system they will be canted at between 76 and 79° from north.

Measurement errors stem primarily from imperfect knowledge of the direction of measurement of each axis and of the contact potential differences. The 2 degree uncertainty in attitude when added to the uncertainties in $\vec{v} \times \vec{B}$ from the trajectory and model magnetic field translates to a 4 mV/m uncertainty in the electric field. Much of the "fatness" of the trace of each component (variations at the spin frequency and its harmonics) is from residual contact potentials. The effort to remove them was stopped after they were no longer the primary source of error. The scatter after 150 seconds in the azimuth of the perpendicular field is a result of the low magnitude of the resultant electric field with the above uncertainties coupled in.

The electric field is initially moderately large and variable ($\sim$ 60 mV/m) and directed northerly, perpendicular to contours of invariant latitude. Note in comparison of Figures 4 and 6 that the small drops in electric field correspond to small rises in particle flux intensity. Near

150 s, correspondent with the large increase in particle flux, the electric field drops abruptly to less than 10 mV/m. As the particle flux is reduced and the rocket passes out of the visual aurora at about 230 s a small increase in field magnitude occurs (the electric field tracks the Pedersen conductivity very well: see Evans et al., 1976). Late in the flight the direction of the perpendicular electric field shifts to a nearly pure westerly direction. This was about the time that the rocket entered the second form.

The direction of the electric field at each edge of the main arc was rotated toward the west by more than 20° from the northerly direction (nearly perpendicular to contours of invariant latitude) seen south of the arc, while in the central part of the arc the direction was again nearly perpendicular to contours of invariant latitude. Between the two arcs the direction was primarily the same as at the edges of the main arc, with a short period at the center of the expanse where the field returned to its initial northerly direction.

The measured electric field parallel to $\vec{B}$ is at all times less in magnitude than $\pm$ 4 mV/m. Since this is less than the uncertainties from the attitude solution and contact potential variations, we conclude that there is no evidence of any parallel electric field.

VII. Discussion

A. Convective Topology

In order to put these measurements in perspective with patterns of convective flow in the midnight zone, convective velocities are plotted every 10 s along the rocket trajectory in Figure 9. The coordinates are

geographic with contours of invariant latitude at 110 km included for reference. Also plotted is the position of the lower border of the aurora as seen in the 240 s photograph shown in Figure 1 (the shaded area does not define the extent of the arc; it only shows on which side of the lower border that the luminosity exists). The trajectory points are the position of its field line at 110 km intersecting the trajectory at the specified time. The auroral lower border was also assumed to be at 110 km for this plot. In scaling the all sky photos, the magnitude of the look angles were calibrated using the star background. The position of the northerly part of the form is subject to large uncertainties due to the low inclination angle. Note, as stated previously the aurora moved southward during the flight and the northerly part of the form was entered at approximately 380 s.

The observed convective flow is towards dusk or "sunward" from the northerly electric field direction consistent with the positive bay condition that was flown into (i.e. Heppner 1972; Wescott et al., 1969; Cauffman and Gurnett, 1972). Near the end of the flight the rotation to the westward electric field or southward convection could have resulted from one of the following: (1) the boundary region separating the auroral zone from the polar cap was entered, (2) the boundary region separating the positive and negative bay regions called the Harang discontinuity (see Maynard, 1974) was entered, or (3) a local eddy structure which may or may not have been related to one of the above was entered. From comparing the magnetograms and the auroral morphology with the data, the most probable conclusion seems to be that the rotation is associated with the Harang discontinuity although the others can not be positively

ruled out. Thus, while the main arc is in the positive bay region, the curling back of the arc would appear to be associated with the Harang discontinuity.

B. Parallel Electric Fields

The existence of field aligned potential drops as an acceleration mechanism for auroral particles is widely accepted and models employing such occasionally have been successful in reproducing measured auroral electron spectra (see Evans, 1974). In what region and over what spatial extent these potential drops exist has been a primary source of controversy. In all of the Ba^+ release measurements both post and pre midnight, no evidence of parallel fields in the ionosphere have been seen (i.e. Mende, 1968; Wescott et al., 1969; Scholer and Haerendel, 1971). Large magnitude parallel electric fields (20 mV/m) have been deduced from double probe measurements on three flights into the post magnetic midnight region. In each case the authors involk anomalous resistivity arguments to prevent the ionosphere from collapsing. Two of these flights involved a single axis measurement in which a constant electric field was assumed along $\vec{B}$ for a "long" ($\sim$ 100 s or more) period and the magnitude adjusted to remove precessional variations in the data (1. Mozer and Bruston, 1967, and Mozer and Fahleson, 1970; 2. Kelley et al., 1971). The third flight involved a two axis measurement capable of resolving all three components every 1/2 spin cycle and detected a parallel field varying between 15 and 27 mV/m between 105 and 310 s and decaying to zero for the last 100 s of flight (Kelley et al., 1975). A Ba^+ release from the same rocket did not see a parallel field. All of these large parallel fields have been directed

downward. Whalen et al. (1975) measured ion velocities in both directions along the magnetic field in a negative bay (at different times during a flight) of 2 km/s from which they deduced, using collision frequencies derived from Coulomb interactions, a parallel field of 0.1 mV/m.

The measurements reported here set an upper limit of ± 4 mV/m on the D.C. parallel electric field during the flight. Since this is within the uncertainties of the measurement we find no evidence of large-magnitude parallel electric fields in the ionosphere below 242 km. It should be noted that this flight was into a relatively stable positive bay auroral condition.

C. Auroral Electron-Electric Field Relationships

Although the detailed electrodynamical relationships between the auroral particles and the electric fields in this auroral arc will be treated in the companion paper (Evans et al., 1976), two general points on these relationships need to be made here. First, a definite anti-correlation of particles and electric fields is observed during this flights' passage over the strong discrete auroral form located inside the "sunward" convecting positive bay region (compare Figures 4 and 8). Such anticorrelation has been observed on many previous flights although it should not be expected in all cases (see discussion in Maynard et al., 1973).

Inverted V precipitation events have been associated with auroral arcs (Ackerson and Frank, 1972) and with electric field reversals at or near the 40 keV trapping boundary (Frank and Gurnett, 1971; Gurnett and Frank, 1973). Auroral arcs have also been associated with electric

field reversals (Swift and Gurnett, 1973). A tendency to reverse the implications of these relationships has subsequently resulted: i.e. all auroral arcs are inverted V events. This is clearly not necessarily true as evidenced by the present study. Burch et al. (1976) using AE-C satellite data have again associated inverted V events with electric field reversals from sunward to antisunward convection or with regions of antisunward convection (in the case of weak events). The second precipitation event observed in this flight having characteristics of an inverted V is located at the convection boundary that we are interpreting as the Harang discontinuity.

Thus, we conclude that auroral arcs totally immersed in the evening sunward convection region are likely not to be associated with inverted V structures. Auroral arcs that occur on convection boundaries, poleward of convection boundaries or in eddy structures associated with convection boundaries are likely to be associated with inverted V events.

Acknowledgments

We gratefully acknowledge the efforts of T. Gerhardson in the design of the gyroscopic reference system and B. Narheim who integrated the rocket. We also acknowledge the financial support of the Royal Norwegian Council for Scientific and Industrial Research, the National Aeronautics and Space Administration and the National Oceanographic and Atmospheric Administration in this joint Norwegian-U.S. program.

References

Ackerson, K. L., and L. A. Frank, Correlated satellite measurements of low-energy precipitation and ground based observations of a visible auroral arc, J. Geophys. Res., 77, 1128, 1972.

Aggson, T. L., Probe measurements of electric fields in space, in Atmospheric Emissions, edited by B. M. McCormac and A. Omholt, p. 305, Van Nostrand Reinhold, New York, 1969.

Burch, J. L., S. A. Fields, W. B. Hanson, R. A. Heelis, R. A. Hoffman and R. W. Janetzke, Characteristics of auroral electron acceleration regions observed by Atmosphere Explorer C, J. Geophys. Res., in press, 1976.

Cauffman, D. P., and D. A. Gurnett, Satellite measurements of high latitude convection electric fields, Space Sci. Rev., 13, 369, 1972.

Chen, A. J., and G. Rostoker, Auroral-polar currents during periods of moderate magnetospheric activity, Planet. Space Sci., 22, 1101, 1974.

Eather, R. H., and S. B. Mende, Airborne observations of auroral precipitation patterns, J. Geophys. Res., 76, 1746, 1971.

Evans, D. S., Precipitating electron fluxes formed by a magnetic field-aligned potential difference, J. Geophys. Res., 79, 2853 1974.

Evans, D. S., N. C. Maynard, E. Maehlum, J. Trøim and A. Egeland, Auroral vector electric field and particle comparisons: 2. Electrodynamics of an arc, to be submitted to J. Geophys. Res., 1976.

Frank, L. A., and K. L. Ackerson, Observations of charged particle precipitation into the auroral zone, J. Geophys. Res., 76, 3612, 1971.

Frank, L. A., and D. A. Gurnett, Distributions of plasmas and electric field over the auroral zones and polar caps, J. Geophys. Res., 76 6829, 1971.

Gurnett, D. A., and L. A. Frank, Observed relationships between electric fields and auroral particle precipitation, J. Geophys. Res., 78, 145, 1973.

Gustafsson, G., and A. Egeland, Auroral emissions in relation to low energy electron flux in the nightside auroral oval, J. Atmos. Terr. Phys., 1976 (in press).

Heppner, J. P., Electric field variations during substorms: OGO-6 measurements, Planet. Space Sci., 20, 1475, 1972.

Hoffman, R. A., and D. S. Evans, OGO-4 auroral particles experiment and calibrations, Goddard Space Flight Center preprint X-611-67-632, 1967.

Kelley, M. C., F. S. Mozer, and U. V. Fahleson, Electric fields in the nighttime and daytime auroral zone, J. Geophys. Res., 76, 6054, 1971.

Kelley, M. C., G. Haerendel, H. Kappler, F. S. Mozer, and U. V. Fahleson, Electric field measurements in a major magnetospheric substorm, J. Geophys. Res., 80, 3181, 1975.

Maynard, N. C., Electric field measurements across the Harang discontinuity, J. Geophys. Res., 79, 4620, 1974.

Maynard, N. C., A. Bahnsen, P. Christophersen, A. Egeland and R. Lundin, An example of anticorrelation of auroral particles and electric fields, J. Geophys. Res., 78, 3976, 1973.

Mende, S. B., Experimental investigation of electric fields parallel to the magnetic field in the auroral ionosphere, J. Geophys. Res., 73, 991, 1968.

Mozer, F. S., and P. Bruston, Electric field measurements in the auroral ionosphere, J. Geophys. Res., 72, 1109, 1967.

Mozer, F. S., and U. V. Fahleson, Parallel and perpendicular electric fields in the auroral ionosphere, Planet. Space Sci., 18, 1563, 1970.

Rees, M. H., and D. Luckey, Auroral electron energy derived from ratio of spectroscopic emissions. 1. Model computations, J. Geophys. Res., 79, 5181, 1974.

Scholer, M., and G. Haerendel, Ambipolar diffusion along magnetic field lines in the presence of a current, Planet. Space Sci., 19, 2759, 1971.

Swift, D. W., and D. A. Gurnett, Direct comparison between satellite electric field measurements and visual aurora, J. Geophys. Res., 78, 7306, 1973.

Wescott, E. M., J. D. Stolarik, and J. P. Heppner, Electric fields in the vicinity of auroral forms from motions of barium vapor releases, J. Geophys. Res., 74, 3469, 1969.

Whalen, B. A., H. J. Verschell and I. B. McDiarmid, Correlations of ionospheric electric fields and energetic particle precipitation, J. Geophys. Res., 80, 2137, 1975.

Figures

Figure 1 - All-sky photos from the range at Andøya showing the aurora at 40, 240 and 440 seconds into the flight. The 110 km intercepts of the magnetic field lines which pass through the rocket at 150 and 230 seconds are shown on the middle photo and that of 380 seconds is shown on the bottom photo.

Figure 2 - Magnetometer records from observatories at Tixie Bay, Dixon Island, Murmansk and Tromsø and from the range at Andøya. The locations of the stations are shown in magnetic local time and invariant latitude at the time of the flight in the polar plot at the upper right. The horizontal magnetic disturbances are shown also from the four observatories (zeros taken from quiet data). The line from Andøya depicts the horizontal extent of the trajectory of Polar 3.

Figure 3 - Onboard photometer records of the auroral intensity of the O1 (6300Å) and N_2^+ (4278Å) emissions. Time is in elapsed time from launch.

Figure 4 - The rate of energy deposition into the atmosphere due to electron precipitation during the flight. These rates were corrected for backscattered electrons by using the responses of the downward viewing detector pair.

Figure 5 - A typical electron energy spectrum observed over the center of the auroral form. The precipitating energy flux associated with this spectrum was 40.5 ergs cm^{-2} s^{-1} of which 7 ergs cm^{-2} s^{-1} was backscattered from the atmosphere below. The scatter in data points is of the same scale as the line width.

Figure 6 - Two electron energy spectra taken during the later part of the Polar 3 flight. The spectrum taken at + 396.30 s has been displaced upwards for clarity. The shape of these spectra, the fact that the pitch angle distributions displayed a modest field aligned anistropy, and the monotonic increase in characteristic electron energy over a latitudinal distance of more than 50 km all suggest that the rather weak precipitation observed after + 310 sec was the low altitude signature of an inverted V.

Figure 7 - The contact potentials in equivalent electric field of each axis versus time which were subtracted to obtain the measured value of $\vec{E} + \vec{v} \times \vec{B}$.

Figure 8 - The measured electric field as a function of time. The bottom half shows all three components of $\vec{E}$ in a magnetically oriented coordinate system (see text). The top half shows the total electric field perpendicular to the magnetic field and the azimuthal angle of the electric field vector from north in this system.

Figure 9 - The topography of the convection velocity derived from the electric field measurements and the observed aurora at 240 s. The convection velocities are plotted every ten seconds from the projection along the magnetic field line of the rocket position to the 110 km level. The auroral lower border was assumed to be at 110 km in the scaling from the all-sky cameras. The shading indicates only the side of the lower border to which the aurora exists and not the horizontal extent of the aurora.

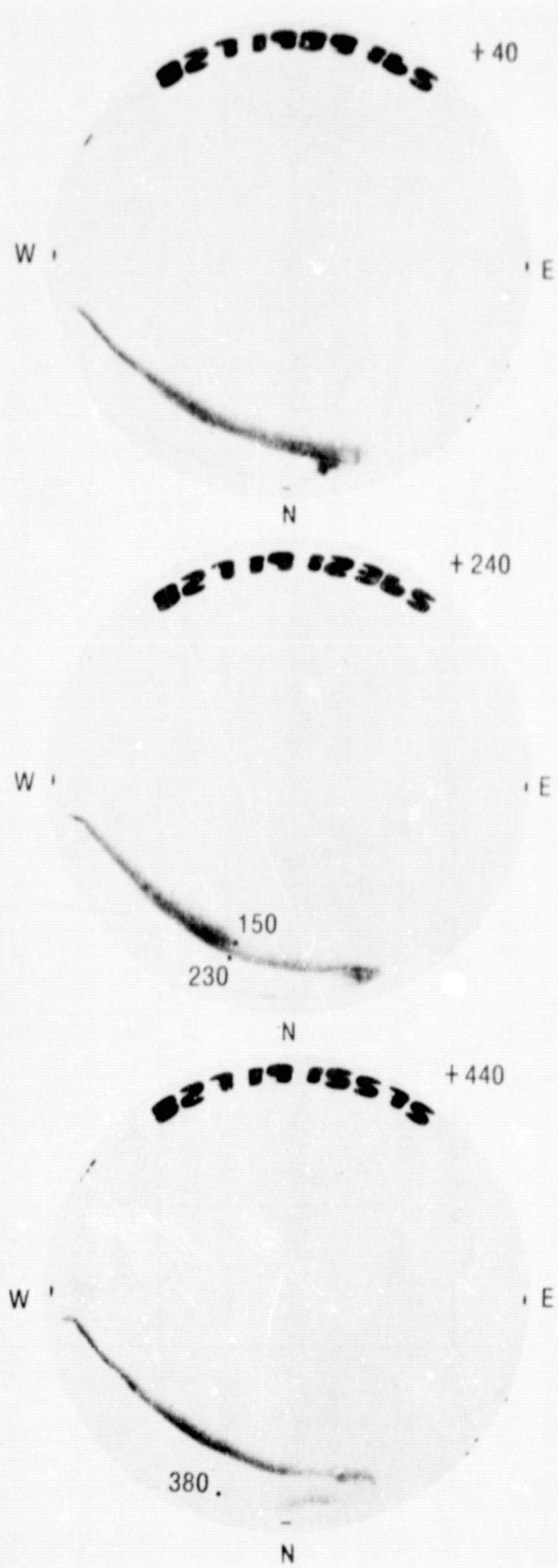

ORIGINAL PAGE IS
OF POOR QUALITY

Figure 1

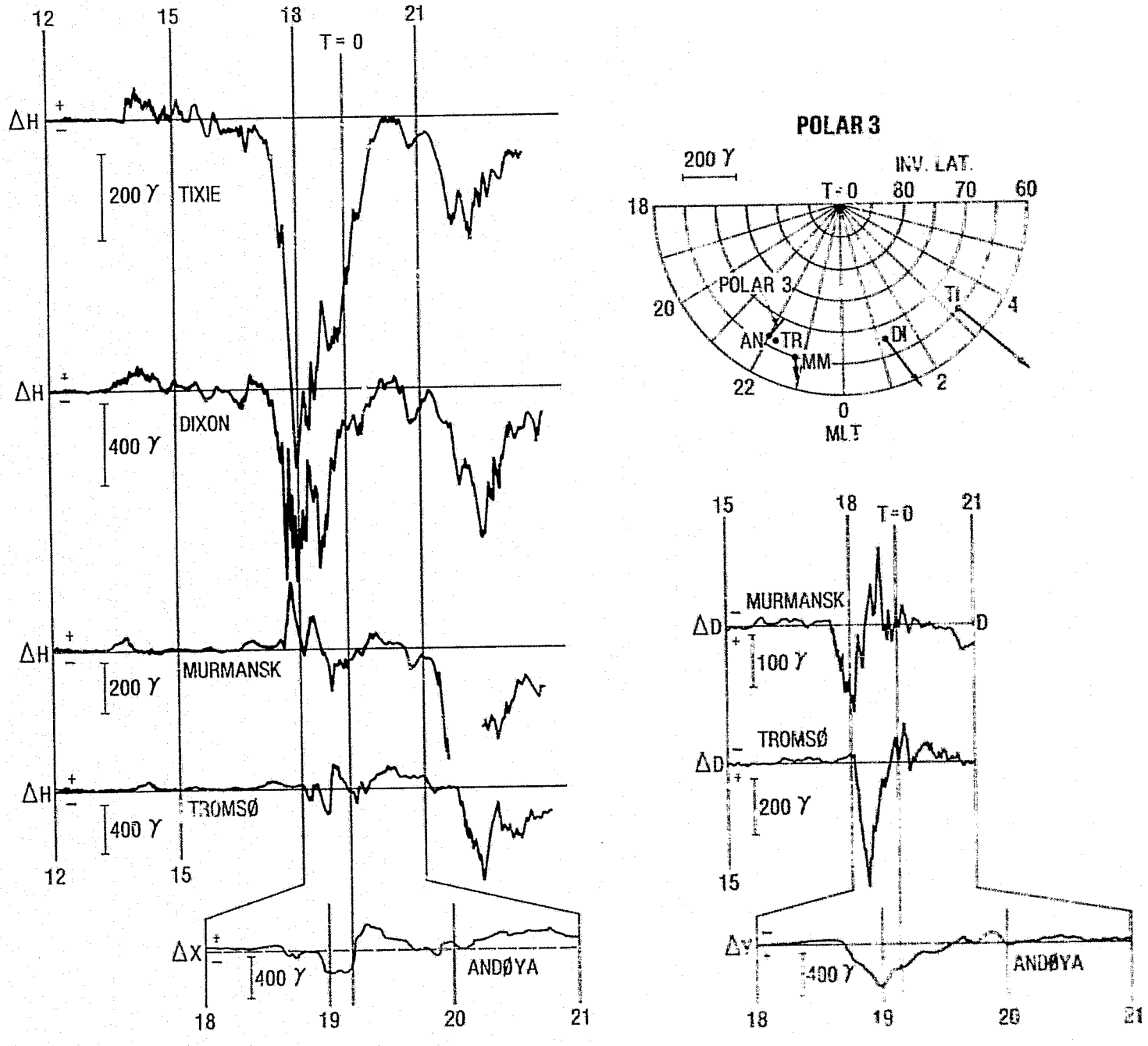
12
15
18
21
T = 0
ΔH
200 γ
TIXIE
DIXON
400 γ
MURMANSK
200 γ
TROMSØ
400 γ
ΔX
ANDØYA
400 γ
18
19
20
21
POLAR 3
200 γ
INV. LAT.
T = 0
80
70
60
18
20
22
0
2
4
MLT
POLAR 3
TI
AN
TR
DI
MM
15
18
T = 0
21
ΔD
MURMANSK
100 γ
TROMSØ
200 γ
ΔY
ANDØYA
400 γ
18
19
20
21

Figure 2

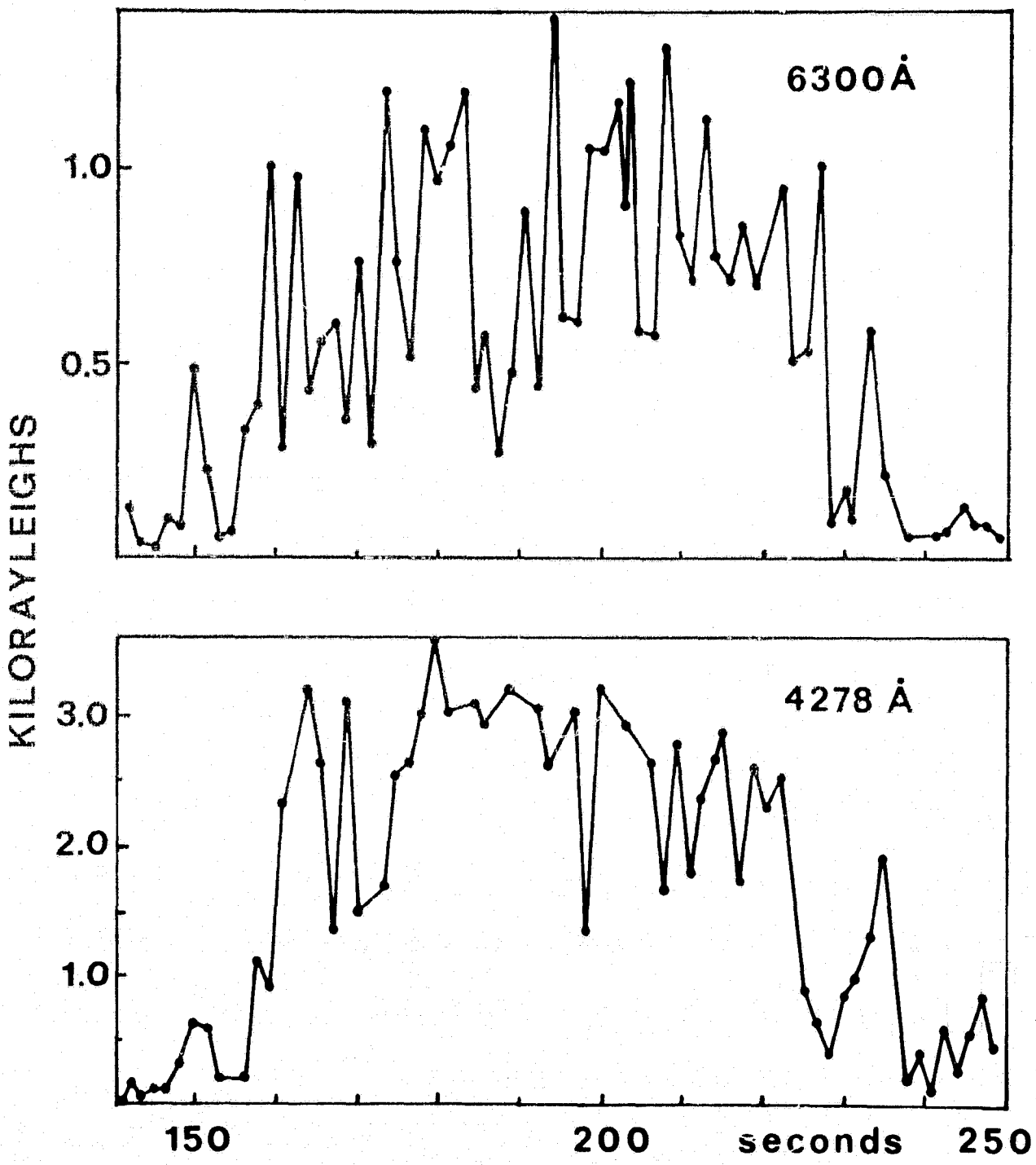

Figure 3

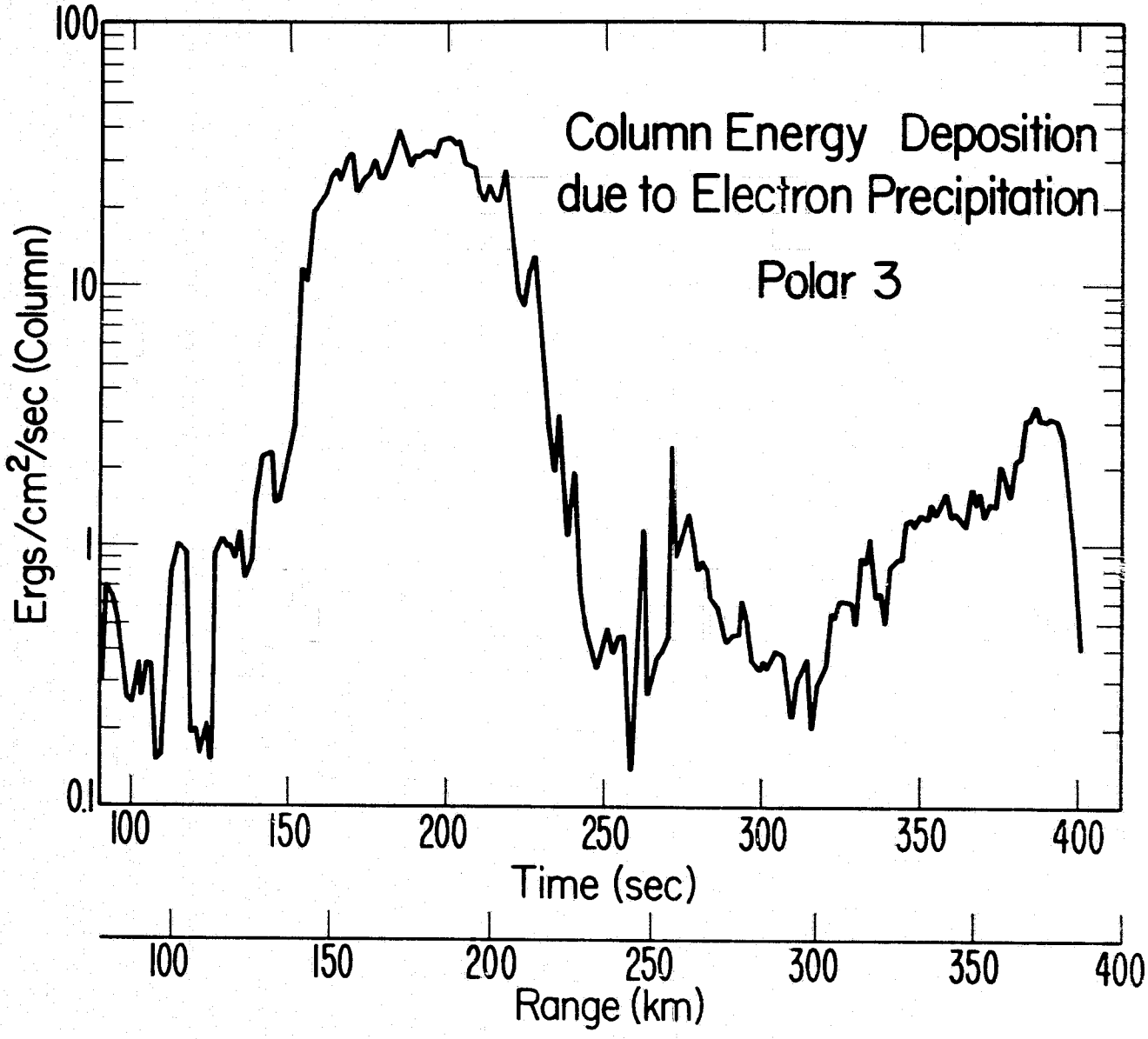
Column Energy Deposition
due to Electron Precipitation
Polar 3
Ergs/cm²/sec (Column)
100
10
1
0.1
100
150
200
250
300
350
400
Time (sec)
100
150
200
250
300
350
400
Range (km)

Figure 4

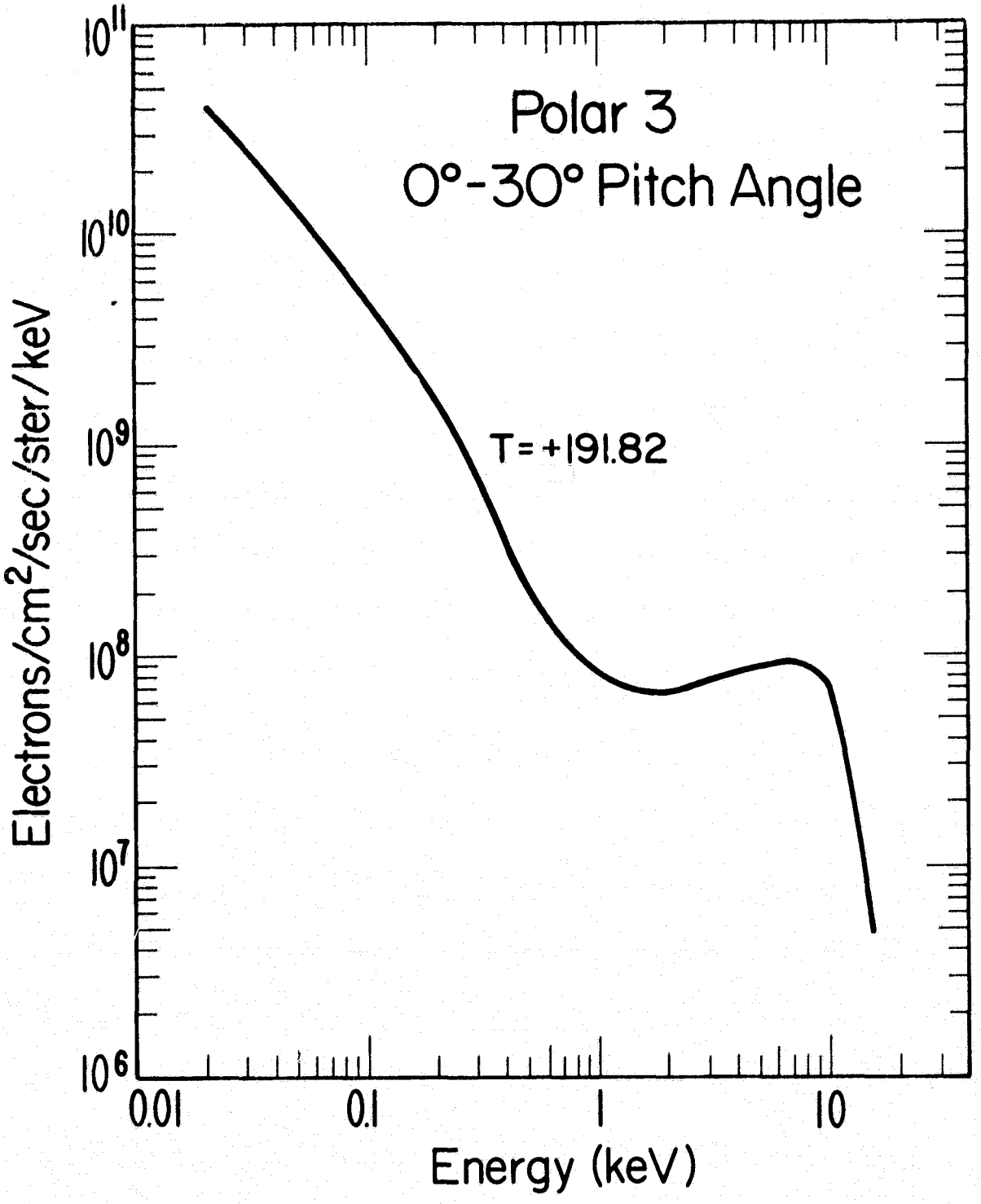
Polar 3
0°-30° Pitch Angle
T= +191.82
Electrons/cm²/sec/ster/keV
Energy (keV)
10¹¹
10¹⁰
10⁹
10⁸
10⁷
10⁶
0.01
0.1
1
10

Figure 5

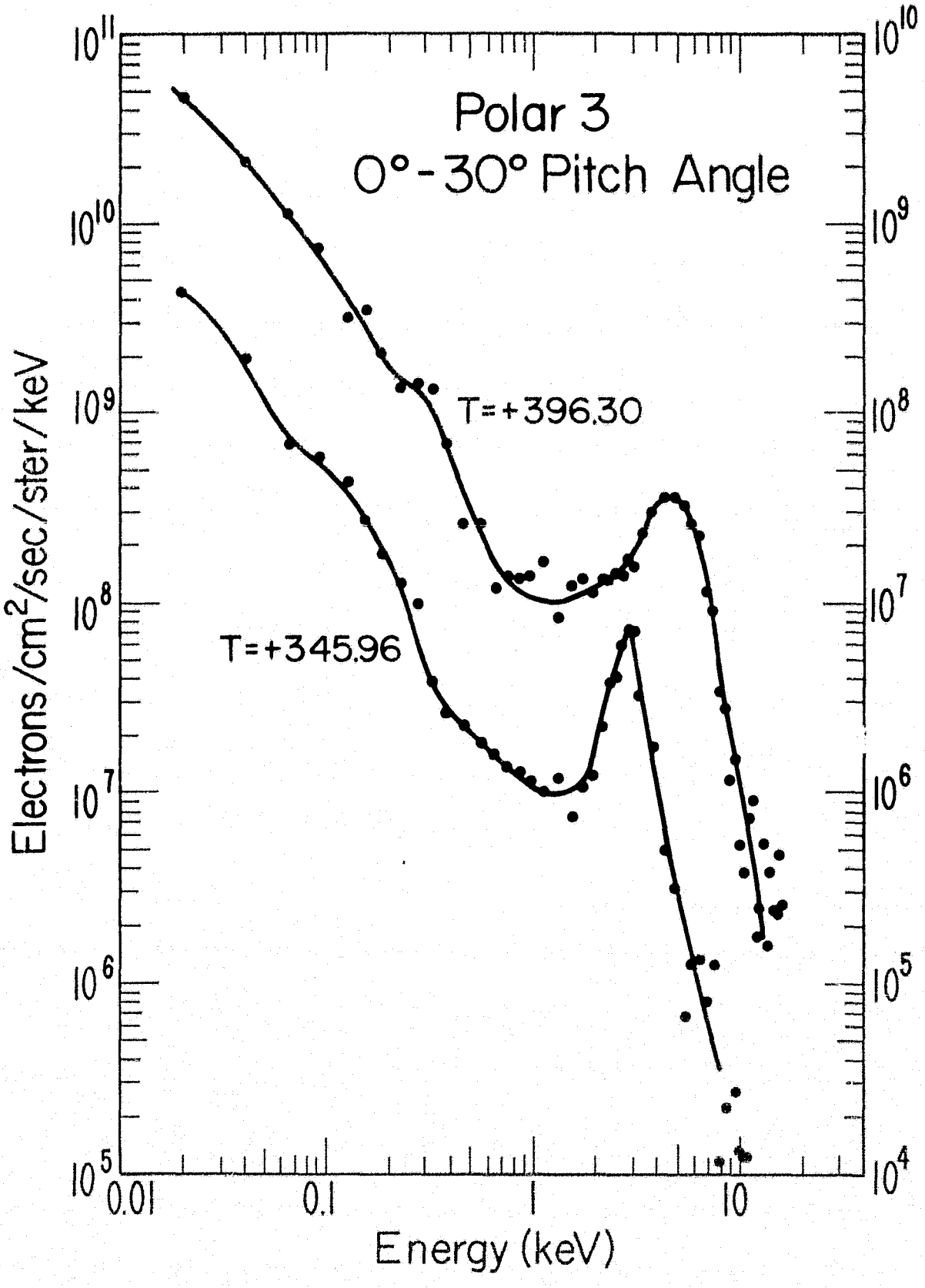
Polar 3
0°-30° Pitch Angle
T=+396.30
T=+345.96
Electrons/cm²/sec/ster/keV
Energy (keV)
10¹¹
10¹⁰
10⁹
10⁸
10⁷
10⁶
10⁵
10⁴
0.01
0.1
1
10

Figure 6

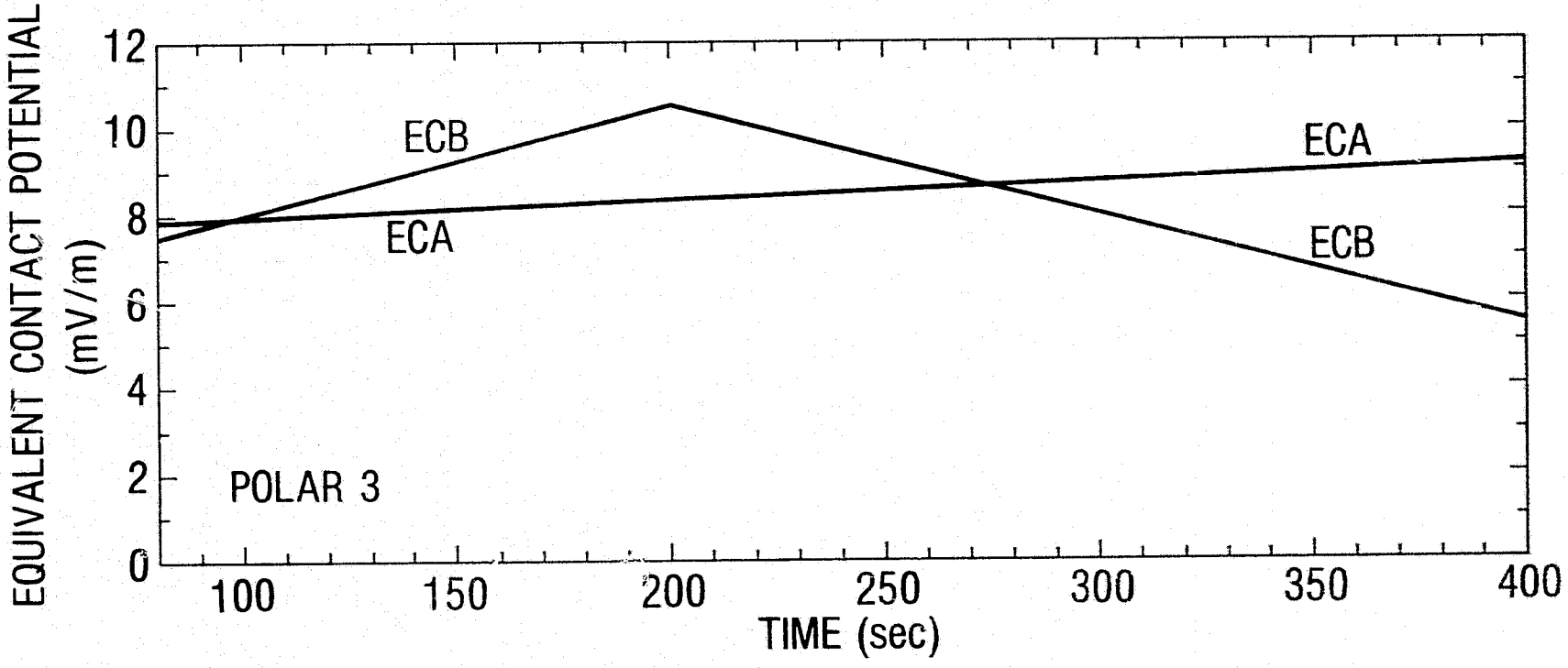
EQUIVALENT CONTACT POTENTIAL
(mV/m)
12
10
8
6
4
2
0
ECB
ECA
ECA
ECB
POLAR 3
100
150
200
250
300
350
400
TIME (sec)

Figure 7

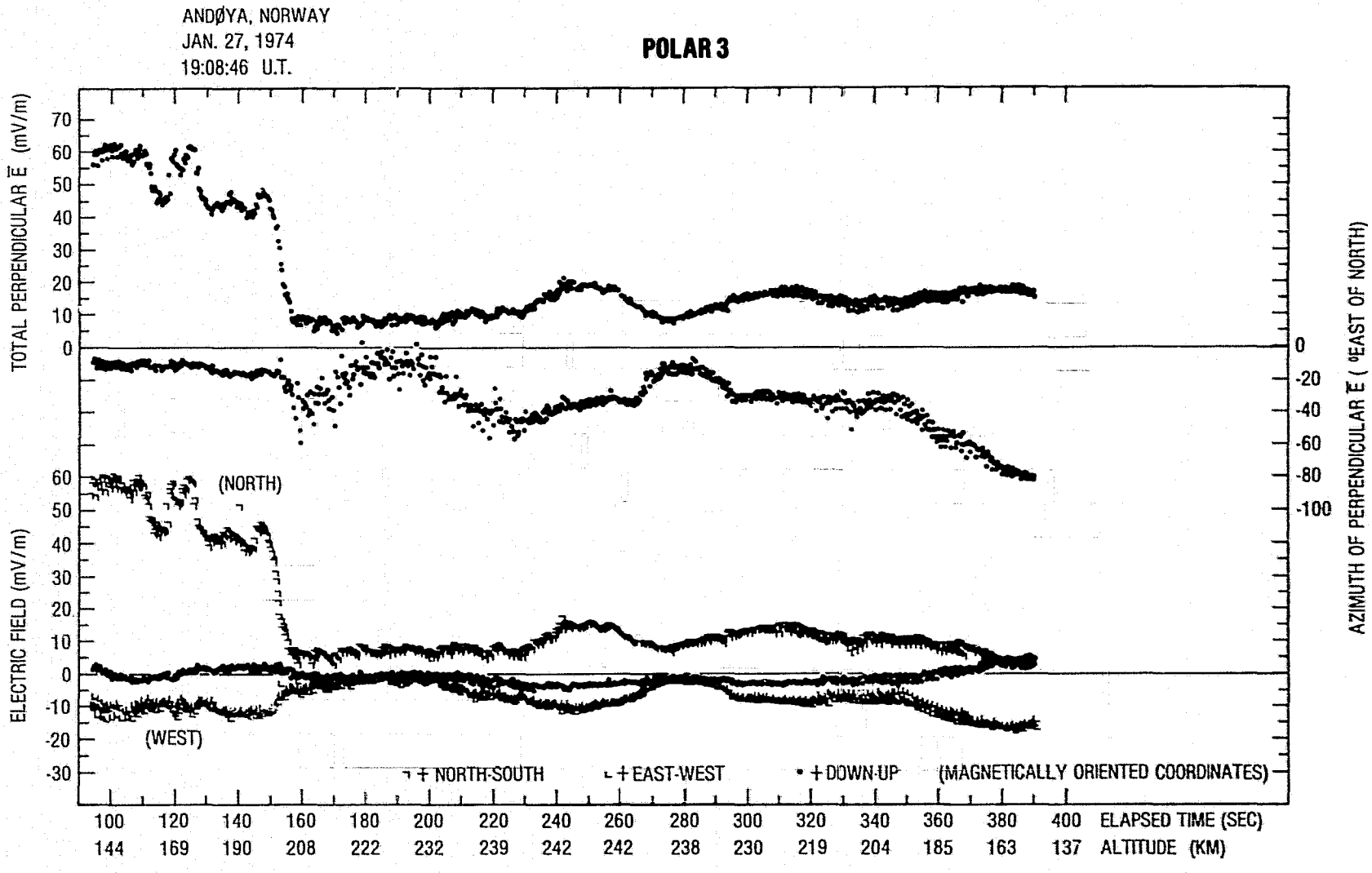
ANDØYA, NORWAY
JAN. 27, 1974
19:08:46 U.T.
POLAR 3
TOTAL PERPENDICULAR Ē (mV/m)
ELECTRIC FIELD (mV/m)
AZIMUTH OF PERPENDICULAR Ē (°EAST OF NORTH)
(NORTH)
(WEST)
+ NORTH-SOUTH
+ EAST-WEST
+ DOWN-UP
(MAGNETICALLY ORIENTED COORDINATES)
ELAPSED TIME (SEC)
ALTITUDE (KM)

Figure 8

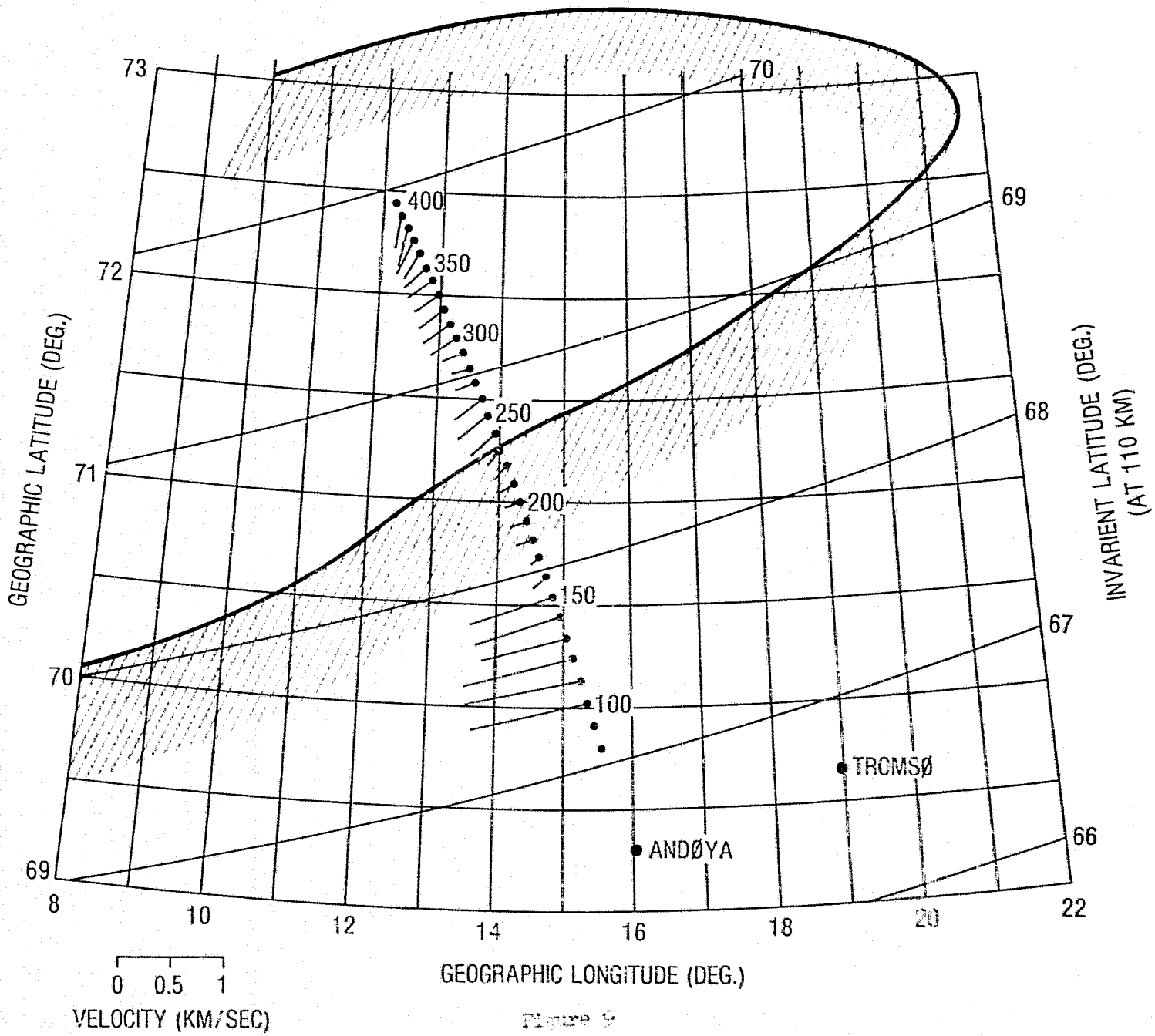
73
72
71
70
69
8
10
12
14
16
18
20
22
70
69
68
67
66
400
350
300
250
200
150
100
TROMSØ
ANDØYA
GEOGRAPHIC LATITUDE (DEG.)
INVARIENT LATITUDE (DEG.)
(AT 110 KM)
GEOGRAPHIC LONGITUDE (DEG.)
0 0.5 1
VELOCITY (KM/SEC)

Figure 9